Journal of Atmospheric and Solar–Terrestrial Physics 263 (2024) 106313

Contents lists available at ScienceDirect

Journal of Atmospheric and Solar-Terrestrial Physics

journal homepage: www.elsevier.com/locate/jastp

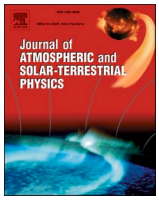

Research Paper

Turbulence, Richardson number (Ri) distributions, and parametric instabilities in the turbopause region (96–105 km) from Na LIDAR measurements at the Andes Lidar Observatory (ALO)

G.R. Swenson [a,*], C.P. Philbrick [b], R.L. Walterscheid [c], J.H. Hecht [d]

[a] University of Illinois at Urbana Champaign, Electrical and Computer Engineering, Urbana, IL, 61801, USA
[b] University of Colorado, Electrical Engineering, Boulder, CO, USA
[c] Embry-Riddle Aeronautical University, Daytona Beach, FL, USA
[d] The Aerospace Corp, Los Angeles, CA, USA

ARTICLE INFO

Handling Editor: Dora Pancheva

Keywords:
Mesosphere
Instabilities
Turbulence
Dynamics
Waves

ABSTRACT

Turbulence in the Mesosphere and Lower Thermosphere (MLT) region is responsible for vertical mixing and transport of constituents and heat and the formation of the turbo-pause. A study of turbulence at the Andes Lidar Observatory (ALO) by Philbrick et al. (2021) found, for 25 nights of lidar observations, the probability of Ri < 1/4 decreased with altitude above 100 km, whereas the power in turbulence increased. The objective of this study is to understand the atmospheric process responsible for the observed increase in turbulence power with altitude. Conventionally turbulence is caused by instabilities due to convection (Ri < 0), and Kelvin-Helmholtz Instabilities (KHI), 0 < Ri < 1/4. These criteria are based on laminar flow, a waveless basic state. However, wave-modulated states requiring Floquet theory may dominate the MLT region and can generate instabilities and turbulence under more stable conditions (Ri > 1/4, Klostermeyer, 1990). It was determined in this study the probability of Ri > 1/4 to be >70% at 105 km, consistent with parametric instability (PI) where large tidal induced wind shears and gravity wave presence are contributing factors.

1. Introduction and background

The turbo-pause is an atmospheric boundary near 100 km, where below the atmosphere is mixed by breaking waves and turbulence; above, constituents are distributed by molecular diffusion. Breaking gravity waves play a major role at these altitudes, causing a stress on the zonal flow that leads to a residual circulation (meridionally) (e.g., Fritts and Alexander, 2003). The associated eddies resulting from breaking waves and instabilities lead to vertical constituent fluxes as well as heat.

This case study investigates lidar observations for the role parametric instabilities may have to conditions leading to turbulence in the MLT region.

1.1. Turbulence, mixing, and diffusion in the MLT

Several studies have made significant contributions to the understanding of instability processes, turbulence, and vertical mixing of constituents and heat. Guo et al. (2017) made spectral measurements of turbulent power versus the vertical wave number (m) and frequency using Na lidar data. The spectral distribution of the power in both the eddy (gravity wave) domain as well as the turbulence region were measured using Na lidar. The turbulence region follows a theoretical and measured distribution of $m^{-5/3}$, and m^{-3} for the eddy domain, for all altitudes between 80 and 100 km. Gardner (2018) describes transport coefficient measurements separately for eddies and turbulence for two ground stations, the Starfire Optical Range (SOR) telescope at Albuquerque, NM and the ALO. His study demonstrated that eddy transport dominated the turbulence process by several factors below 90 km, for both sites, but became equally important near 96 km. The altitude limit of this method is ~100 km.

Bui et al. (2023) cited a number of earlier plasma and neutral instabilities primarily observed with radars. Neutral instabilities, including those described in that study which led to turbulence, are characterized by a convection or Kelvin-Helmholtz instabilities (Ri ≤

* Corresponding author.
E-mail addresses: swenson1@illinois.edu (G.R. Swenson), channing.philbrick@gmail.com (C.P. Philbrick), r.walterscheid@att.net (R.L. Walterscheid), James.H.Hecht@aero.org (J.H. Hecht).

https://doi.org/10.1016/j.jastp.2024.106313
Received 20 January 2024; Received in revised form 10 July 2024; Accepted 18 July 2024
Available online 20 July 2024

1/4) or the parametric condition further described herein. That includes secondary processes such as mesospheric inversion layers (MILS) that result from heated regions due to breaking waves, which produce a near adiabatic lapse rate (and Ri < 0) on the top side of the MILs leading to convection instabilities (Li et al., 2005).

Diffusion of atmospheric constituents is accomplished by molecular processes where collisions dominate and eddy processes where mixing dominates. The parameterization of effective eddy diffusion coefficients (k_{zz}) has been deduced from the vertical distributions of O densities whose distribution with altitude and eddy flux is determined from known chemical loss processes. Swenson et al. (2021) describes the intra-annual variation of k_{zz} (for all overturning processes) as described by atomic oxygen climatologies for 18 years of the NASA TIMED SABER and 10 years of the ENVISAT SCIAMACHY measurements. The vertical transport of minor constituents includes atomic oxygen, where the reservoir maximum density is at an altitude of ~97 km. The upper limit of the method using OH airglow emissions from SABER is ~96 km and O (^{1}S) airglow from SCIAMACHY is ~105 km (Swenson et al., 2021).

The region between 80 and 100 km has been well studied due to the plethora of remote sensing tools including lidar and airglow. However, the region above has been sparsely sampled, primarily due to low densities of metals (Na, Fe, K) used for lidar resonance as well as weak chemiluminescent airglow emissions.

1.2. Theory of instabilities and the Richardson number

Conventionally, the classical criteria used to predict the onset of instability are based on laminar flow. Atmospheric instabilities, which can lead to the onset of turbulence, are characterized by the Richardson number (Ri) and Brunt-Väisälä frequency (N). The Brunt–Väisälä frequency squared

$$N^2 = \frac{g}{C_p}\left(\Gamma_{ad} + \frac{\partial T}{\partial z}\right) \quad (1)$$

is the parameter relevant to convective stability where g is gravitational acceleration, $\partial T/\partial z$ is the atmospheric lapse rate, Cp specific heat, Γ_{ad} is the adiabatic lapse rate (~9.5 K/km).

Convective instability occurs when $N^2 < 0$. Kelvin–Helmholtz Instabilities (KHI, associated with vertical wind shear) are characterized by the Richardson Number (Ri), which is defined as the ratio of N^2 to the square of the vertical shear of the horizontal wind (S^2) and is given by

$$Ri = \frac{N^2}{(\partial U/\partial z)^2 + (\partial V/\partial z)^2} = \frac{N^2}{S^2} < \frac{1}{4} \quad (2)$$

where U is the zonal and V the meridional wind components (Richardson, 1920). The region where $0 < Ri < 1/4$ is a necessary but not sufficient condition for KHI formation.

1.3. Floquet theory and PI

In Floquet theory the stability of a wave (primary wave) on a wave-disturbed background (the Floquet wave) is examined. The occurrence of parametric instability (PI) and its growth rate depend on the amplitude of the primary wave and on the extent to which a third wave satisfies conditions for a resonant triad interaction involving the primary wave and the Floquet wave [Klostermeyer, 1990]. Instabilities of a KHI type in this system can occur at Richardson numbers significantly greater than the laminar value of ¼.

Tides should play a role in inducing PI. In simplest terms, one would expect the tides to modulate the intrinsic frequencies involved in PI triad interactions and shift some interactions toward PI and others away. However, the process is not symmetric; waves that are swept up in instability are lost. Those that are not lost at one time are still subject to instability at another. That is, there should be a bias toward increased instances of instability. Tides, planetary waves, and gravity waves are all, ever present wave features in the MLT region, conditions favorable to the production of PI.

Walterscheid et al. (2013) studied instability structures in the 84–92 km region airglow and used Na lidar measurements to determine winds and temperatures. Those observations were used to determine the Ri, where the turbulence was observed in the presence of the Ri > 1/4. They described those conditions as Floquet wave conditions (PI). In that study, turbulence was associated with $0 < Ri < 1$.

Philbrick et al. (2021) analyzed lidar data for the power in the turbulence spectra to 105 km altitude, where the distributions of the Ri were determined to be consistent with parametric instability process domination. The existence of turbulence in regions where Ri > 1/4 implies that instabilities must also be present in those regions due to Taylor's frozen-in hypothesis, a condition that assumes turbulent eddies are advected by the mean flow velocity, without changes in their properties, and that by process of elimination those instabilities must be solely due to parametric instabilities. P21 used a method that characterized the spatial distributions in the Na lidar returns, enabling the method to reach 105 km with an equivalent S/N to that which the Doppler method (e.g., Gardner, 2018) would have at 96 km. P21 analyzed 25 nights from the Andes Lidar Observatory (ALO) in Cerro Pachón, Chile, which were used to determine the power in turbulence, and a value of $k_{zz,turbulence}$ versus altitude. This work describes the analysis leading to this result, including the distribution of the conditional probability of the Ri.

2. Analysis

P21 described an analysis of 25 nights of lidar data from the ALO. Turbulence was extracted from the spatial distribution of Na density perturbations rather than the traditional Doppler methods (e.g., Gardner, 2018), to an altitude of 105 km. P21 found the probability of instabilities due to convection and KHI (Ri < 1/4) decreased above 100 km while turbulence power increased (Fig. 1). The objective of this study is to deduce the cause of the increased turbulence.

2.1. Determination of Ri distributions from lidar P21 and W13

The data used by W13 was determined from an OH airglow imager, operating at 1.6 μ m, that was located on Mt. Haleakala, Maui, HI, where there was also a co-located Na lidar. The lidar was the same one that was later relocated to Cerro Pachon, Chile. They analyzed data for 13 nights between 2002 and 2005. The OH images were used to measure turbulence and its isotropicity with respect to the winds and the Na lidar data provided the information to compute Ri. Turbulent conditions were deduced from 'ripples' in the OH images. Wavelet analysis was performed on images characterizing primary wave and secondary (ripple) structure. A phase correlation method was used to determine the apparent drift direction and phase velocity of ripples with respect to the primary wave. Since ripples due to KHIs drift with the wind, the drifts correlated with the primary waves were consistent with parametric instabilities.

The data used by P21 was collected in 25-m altitude increments and binned to 250-m increments, with a new profile measured every 6 s. Each of the 25 nights in the dataset contained measurements of horizontal wind, where the lidar was pointed in a zenith-south-zenith-east (ZSZE) sequence with the look direction updated every 78 s. While horizontal wind measurements were necessary for correlating the $k_{zz,turbulence}$ profiles against Ri measurements, the 78-s integration time imparted by the ZSZE pattern limited observations to a portion (between 13 mHz and 83 mHz) of the full turbulence subrange such that the spectrum from N (~3 mHz) to 13 mHz was not characterized. The temperature and horizontal wind profiles, from which N and Ri were produced, were calculated at 500-m, 160-s resolution and smoothed with a 1000-m, 30-min window.

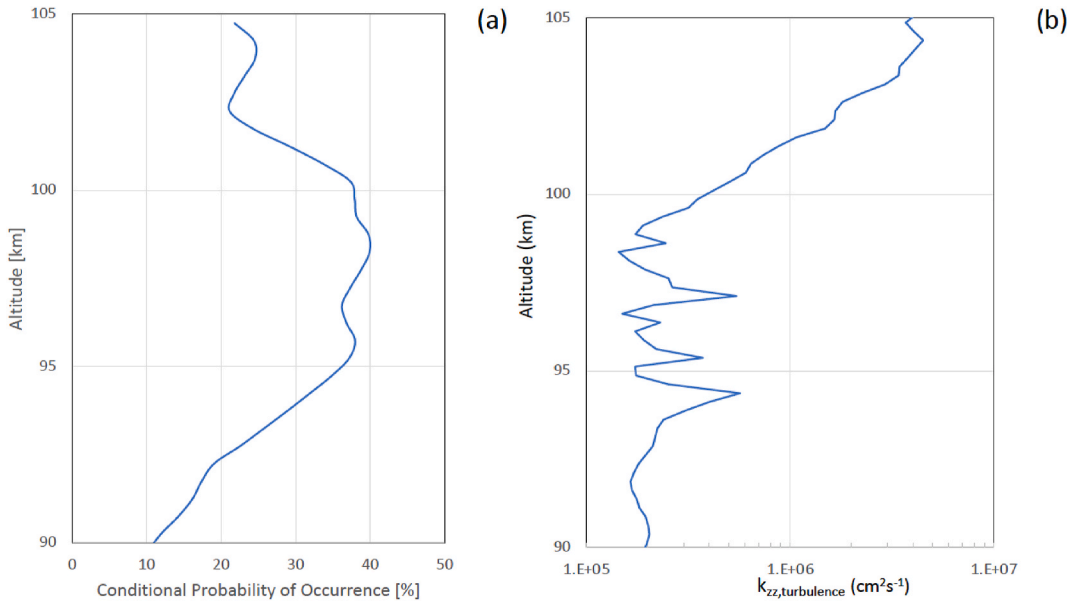

Fig. 1. (a) A plot of the probability of the occurrence (for observed turbulence conditions) of the Richardson number being less than ¼ versus altitude, and (b) the eddy diffusion coefficient for turbulence only ($k_{zz,turbulence}$) versus altitude for lidar data analyzed by P21. Note the probability decreases from ~40% at 100 km to ~25% at 105 km. The power in turbulence (not shown), which is linearly related to $k_{zz,turbulence}$ (shown in b), increases ~1 order of magnitude over the same altitude range.

3. Results

3.1. Comparison of W13 and P21 results

The Richardson number distribution for the probability of observed turbulence, above 100 km from P21 is described in Fig. 2, where it is compared with the distribution measured by W13 for conditions of parametric instability.

The W13 measurements shown include wave induced instability structures (ripples) only. Instabilities advected with the mean flow, were eliminated. Observations of OH airglow structure (ripples) were used to discriminate the direction of the drift of ripples, for lidar measured wind directions. The P21 distributions for conditions of turbulence shown in Fig. 2 have 70% greater than Ri < 1/4. The P21 data includes all turbulence processes, since the lidar measurement method can't resolve the process producing it.

The probability of occurrence of 0 < Ri < 1 versus altitude was further analyzed from the P21 data set and is plotted in Fig. 3. The PI is essentially a KHI condition modified by the presence of waves to occur under more stable atmospheric conditions, and the presence of waves and their amplitude versus altitude also contributing to the PI.

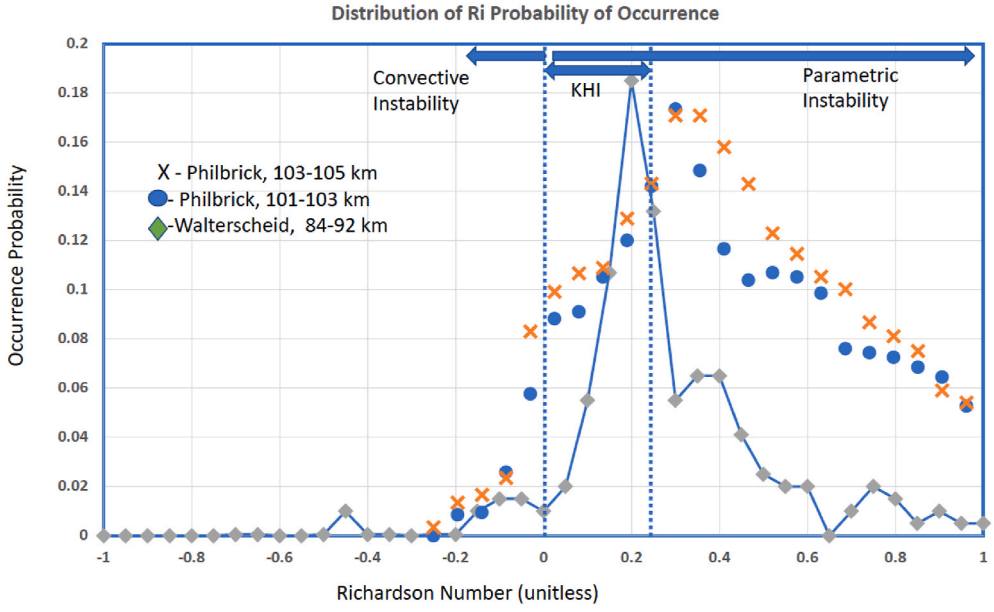

Fig. 2. The conditional occurrence probability versus the Ri for P21 for 101–103 km altitude (circles) and 104–105 km altitude (x's) for measurements at the ALO, and for W13 measurements for 84–92 km altitude measurements made at Maui, HI (diamonds and solid line). The vertical dotted lines at Ri = 0 and ¼ bound convection instability (Ri < 0) and KHI (0 < Ri < 1/4).

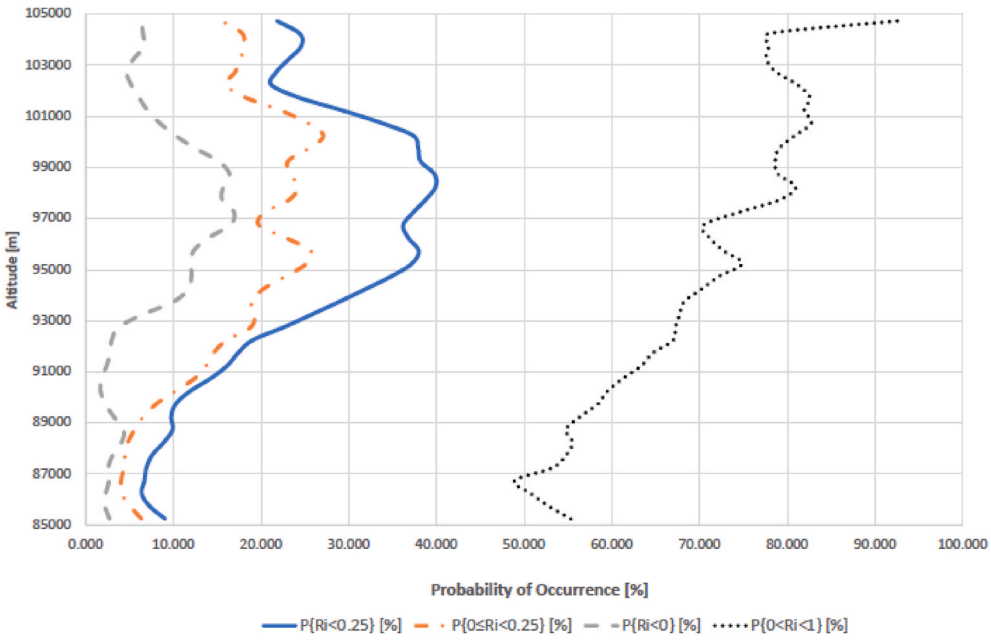

Fig. 3. The probability of occurrence of Ri < 0.25, 0 < Ri < 0.25, Ri < 0, and 0 < Ri < 1 versus altitude for the condition the lidar dataset described in P21. Note that Ri < 1/4 vs altitude shown in Fig. 1 is decreasing above 96 km, whereas the 0 < Ri < 1, the condition for PI, is relatively constant 98 < z < 104.

4. Discussion of results

The distribution measured by W13 (Fig. 2) for Ri > 0 was attributed to parametric instabilities when waves modulate the background state seen by other waves. Earlier measurements of the phenomena were investigated by Klostermeyer (1990) as well as others. The altitude region below 96 km is well understood to be dominated by breaking waves (Gardner, 2018).

The distribution of P21 above 100 km (Fig. 2), where the Ri > 1/4 for more than 70% of measurements, is consistent with parametric instabilities, similar to that analyzed by W13. Note the P21 distribution for Ri > 1/4 is significantly larger than the W13 measured distribution for parametric instabilities. The most probable value for the W13 distribution is ~Ri = 0.2 and for P21 is ~Ri = 0.3. The larger distribution of Ri > 0.25 in P21 is likely due to the increased shear associated with the tides as a function of altitude (Larsen, 2002; England et al., 2022). A statistical study of ALO data by Yang and Liu (2022, Figure7) described background shears increasing a factor of 2 (4× in shear^2) between 95 and 100 km, effectively decreasing Ri over the same altitude region. Their analysis demonstrated the largest contributions from wave effects on the Ri at the upper limit of their data (100 km). We note the W13 distribution of Ri for parametric instabilities does contain a significant distribution for 0 < Ri < 1/4, the classical range for KHI, though it should be noted that parametric instabilities operate in this range as well. The fact that the distribution of the Ri > 1/4 for P21 is significantly larger than W13, suggests that the parametric process shifts in the presence of larger shears (at higher altitudes).

It is recognized that the presence of turbulence with altitude described in Fig. 1 results from two conditions, one being the Floquet wave enhanced KHI stability condition (PI), represented by the Ri, and two, the presence and amplitudes of waves to cause instability. Uniquely, the condition of PI is the likely cause of the increased power in turbulence above 100 km, described by P21.

We recognize that wave mixing also plays a significant role in vertical mixing, a physical process not described by instabilities, and the Ri (Gardner et al., 2022). Those contributions to the region above 100 km are yet to be determined, as well as the potential that wave mixing and parametric instabilities are one and the same.

An investigation of the spectra of eddies and turbulence (from Nyquist limit to N and from N to the inner scale of turbulence, respectively; see Guo et al., 2017) for the conditions where parametric instability is prolific is warranted. It is noted here that the P21 analyzed the power and determined a turbulence only $k_{zz,turbulence}$ (Fig. 1 b) which is a lower limit for the P21 data. It is left to a follow-on study to establish the measurements of the spectra. The prevalence of ripples due to parametrically induced KHI can be inferred from airglow. In the 84–92 km altitude region, W13 measured the occurrence of ripples in the OH airglow images. Airglow images are available near 96 km in OI (^{1}S, 557 nm) airglow that may provide some information.

It is also relevant to point out the very large $k_{zz,turbulence}$~400 m^{2}s^{-1} measured by lidar (Fig. 1 b) at 105 km described by P21 is similar to the $k_{zz,total}$ deduced from the SCIAMACHY instrument measurements described by Swenson et al., (2021). The point is, given the large values (albeit statistical for one geographical location) being 'turbulence only' suggests that turbulence is likely a dominant process at these upper altitudes relative to the 90 km region, where clearly breaking waves dominate over turbulence (Gardner, 2018).

The observations of the atmospheric state are scales, the lower limit of which is defined by the measurement method. Limb measurements from satellite typically are limited to ~300–500 km scales due to the geometry of the limb tangent method. Na lidar measurements of winds for the Ri using angular methods such as accomplished in the W13 and P21 studies scale to ~10's of km. The correlations of occurrence are for the scale of the measurement, in this case the Ri, for a single location. The study of extensive regions of the atmosphere of the Ri and turbulence using lidar could be employed from aircraft and/or space platforms to provide global information on the MLT. Clearly, the distributions of waves and turbulence varies temporally and spatially, requiring additional measurements to better understand the global atmosphere.

5. Conclusions

The analysis of 25 nights of ALO lidar data indicate that parametric instability dominated over convective and KHI instabilities, above 100 km. The conditional probability of ¼<Ri < 1 (parametric instability) was >70% at 105 km, reinforcing the hypothesis that parametric instability is the likely candidate describing the large $k_{zz,turbulence}$ that

was observed by P21 in the MLT turbopause region. A strength of the study is that the explanation of the power in turbulence departure from traditional (convective and Kelvin-Helmholtz) instabilities is supported by PI, a theoretically sound method.

This is a case study, and should not be construed to be all encompassing to the MLT at all times and locations. A shortcoming of this study is it was performed at a single location. Other locations at all latitudes should be studied, accordingly. Additional (future) analysis of the spectral power in turbulence and overturning from breaking waves is necessary to establish the total vertical transport and eddy diffusion values associated with parametric instabilities.

CRediT authorship contribution statement

G.R. Swenson: Writing – review & editing, Writing – original draft, Visualization, Project administration, Methodology, Investigation, Formal analysis, Conceptualization. **C.P. Philbrick:** Writing – review & editing, Methodology, Investigation, Conceptualization. **R.L. Walterscheid:** Writing – review & editing, Visualization, Investigation, Conceptualization. **J.H. Hecht:** Writing – review & editing, Investigation.

Declaration of competing interest

The authors declare that they have no known competing financial interests or personal relationships that could have appeared to influence the work reported in this paper.

Data availability

This paper analyzes and compares data from two published papers. The permissions from those two publishers are included in the file list.

Acknowledgements

The work at the University of Illinois has been partially supported by the NSF Geosciences Division under the National Science Foundation (NSF) Grant AGS 17-59573. Support for J. Hecht at The Aerospace Corporation was provided by National Science Foundation grant numbers AGS1450660 and AGS1911952. The ALO data incorporated in the P21 study is located at: (http://lidar.erau.edu/data/nalidar/index.php).

References

Bui, M.X., Hysell, D.L., Larsen, M.F., 2023. Midlatitude sporadic E-layer horizontal structuring modulated by neutral instability and mixing in the lower thermosphere. J. Geophys. Res.: Space Phys. 128, e2022JA030929 https://doi.org/10.1029/2022JA030929.

England, S.L., Englert, C.R., Harding, B.J., Triplett, C.C., Marr, K., Harlander, J.M., et al., 2022. Vertical shears of horizontal winds in the lower thermosphere observed by ICON. Geophys. Res. Lett. 49, e2022GL098337 https://doi.org/10.1029/2022GL098337.

Fritts, D.C., Alexander, M.J., 2003. Gravity wave dynamics and effects in the middle atmosphere. Rev. Geophys. 41 (1) https://doi.org/10.1029/2001rg000106.

Gardner, C.S., 2018. Role of wave induced diffusion and energy flux in the vertical transport of atmospheric constituents in the mesopause region. J. Geophys. Res. Atmos. 123, 6581–6604. https://doi.org/10.1029/2018JD028359.

Gardner, C.S., She, C.-Y., Yan, Z.-A., 2022. Seasonal variations of gravity wave induced thermal and constituent diffusivities in the mesopause region above Ft. Collins, CO (40.6°N, 105.1° W). J. Geophys. Res. Atmos. 127, e2021JD036387 https://doi.org/10.1029/2021JD036387.

Guo, Y., Liu, A.Z., Gardner, C.S., 2017. First Na lidar measurements of turbulence heat flux, thermal diffusivity, and energy dissipation rate in the mesopause region. Geophys. Res. Lett 44, 5782–5790.

Klostermeyer, J., 1990. On the role of parametric instability of internal gravity waves in atmospheric radar observations. Radio Sci. 25, 983–995.

Larsen, M.F., 2002. Winds and shears in the mesosphere and lower thermosphere: results from four decades of chemical release wind measurements. J. Geophys. Res. 107 (A8), 1215. https://doi.org/10.1029/2001JA000218.

Li, F., Liu, A.Z., Swenson, G.R., 2005. Characteristics of instabilities in the 302 mesopause region over Maui, Hawaii. J. Geophys. Res. 110, D09S12. https://doi.org/10.1029/2004JD005097, 303.

Philbrick, C.P., Yang, F., Vargas, F., Swenson, G., Liu, A., 2021. A Na density lidar method and measurements of turbulence to 105 km at the Andes Lidar Observatory. J. Atmos. Sol. Terr. Phys., 105642 https://doi.org/10.1016/j.jastp.2021.105642.

Richardson, L., 1920. The supply of energy from and to atmospheric eddies. Proceedings of the Royal Society A 97, 354–373. https://doi.org/10.1098/rspa.1920.0039.

Swenson, G.R., Vargas, F., Jones, M., Zhu, Y., Kaufmann, M., Yee, J.H., Mlynczak, M., 2021. Intra-annual variation of eddy diffusion (k_{zz}) in the MLT, from SABER and SCIAMACHY atomic oxygen climatologies. J. Geophys. Res. Atmos. 126, e2021JD035343 https://doi.org/10.1029/2021JD035343.

Walterscheid, R., Gelinas, L., Hecht, J., Liu, A., 2013. Instability structures during periods of large Richardson number (R>1/4): evidence of parametric instability. J. Geophys. Res. Atmos. 118, 6929–6939. https://doi.org/10.1002/jgrd.50514.

Yang, F., Liu, A.Z., 2022. Stability characteristics of the mesopause region above the Andes. J. Geophys. Res.: Space Phys. 127, e2022JA030315 https://doi.org/10.1029/2022JA030315.